Atomic-Scale Material Removal Mechanisms in CeO_2-Based Chemical Mechanical Polishing of 4H-SiC

Xiaofeng Zou[1], Zheng Liu[1], Wanchao Liu[2], Zhongyang Liu[3], Wenwu Zhang[4] and Zejia Zhao[1,4,*]

[1]*Institute of Semiconductor Manufacturing Research, College of Mechatronics and Control Engineering, Shenzhen University, Shenzhen, 518060, Guangdong, China*

[2]*ZTE Corporation, No. 55, Keji South Road, Nanshan District, Shenzhen, 518057, Guangdong, China*

[3]*The Photonics Center of Shenzhen University, Shenzhen, 518060, Guangdong, China*

[4]*State Key Laboratory of Radio Frequency Heterogeneous Integration, Shenzhen University, Shenzhen, 518060, Guangdong, China*

Abstract: Silicon carbide (SiC), as a third-generation semiconductor material, is widely used in satellite avionics cooling systems and high-power aircraft electronics. Chemical mechanical polishing (CMP) is a critical process for achieving global surface planarization in semiconductors. Understanding the atomic-scale material removal mechanisms in CMP of SiC is crucial for achieving defect-free surfaces in SiC-based devices. This study combines molecular dynamics (MD) simulations with experimental investigations to elucidate the mechanochemical interactions between CeO_2 abrasives and SiC substrates during CMP. Through atomistic MD simulations, we demonstrate how abrasive particle size influences localized temperature elevations, stress distributions, and subsurface amorphization, as well as its potential impact in aerospace thermal environments. The results indicate that abrasives larger than 2 nm (>2 nm) promote dislocation propagation and lattice destabilization. A novel dual-stage polishing method is proposed, which yielding an ultra-smooth surface with an arithmetic mean surface roughness (Sa) of 0.157 nm. Mechanistic insights derived from MD simulations, particularly regarding the dynamic oxidation of SiO_2 and defect-passivated material removal, are experimentally validated, confirming minimal subsurface damage (<1 nm in depth) under optimized abrasive and redox cycling conditions. This work establishes a framework for achieving atomic-level surface perfection in SiC by decoupling material removal rate from surface damage through tailored abrasive design and process parameter optimization. The findings provide essential guidance for non-destructive CMP of ultra-hard semiconductor materials, effectively linking atomic-scale mechanisms to macroscopic surface engineering outcomes. The outcome of this paper is potential for aerospace thermal management systems, including thermal protection systems (TPS) in hypersonic vehicles, satellite avionics, and high-power aircraft electronics.

Keywords: SiC, Material removal mechanisms, Molecular Dynamics simulation, CMP, Surface damage.

1. INTRODUCTION

As a third-generation semiconductor material, silicon carbide (SiC) demonstrates outstanding performance compared to traditional semiconductor materials [1], processing exceptional characteristics such as a wide forbidden band, a high saturation electron drift rate, a high critical breakdown electric field, and high thermal conductivity [2, 3], which is widely applied in aerospace, new energy, and high-power devices [4, 5]. SiC-based ceramic matrix composites (CMCs), particularly C/C-SiC, exhibit excellent structural integrity at elevated temperatures, enabling them to serve as thermal protection and load-bearing structures for the Thermal Protection System (TPS) of supersonic/hypersonic vehicles [6]. Additionally, SiC is extensively used in satellite avionics additionally, SiC is extensively used in satellite avionics cooling systems and high-power aircraft electronics due to its superior heat dissipation capability and resistance to harsh space environments [7]. For example, hypersonic vehicles experience extreme aerothermal loads (heat flux up to 10000 W/m²) during re-entry, requiring TPS materials with both high thermal conductivity and structural stability [8]. SiC power electronics in aircraft engines operate under thermal cycling between -55°C and 200°C, where surface defects can induce stress concentration and accelerate failure [9, 10]. However, challenges including high manufacturing costs and considerable processing difficulties remain to be addressed through further research. To support high-density integrated circuit fabrication in avionics and prevent microscopic defects (e.g., scratches, pits) on the SiC substrate surface from impairing epitaxial layer growth and thermal performance, obtaining an atomically smooth, defect-free, and globally planarized SiC substrate surface is crucial [11-14]. Surface roughness and subsurface damage directly impact heat flux management in

*Address correspondence to this author at Institute of Semiconductor Manufacturing Research, College of Mechatronics and Control Engineering, Shenzhen University, Shenzhen, 518060, Guangdong, China;
E-mail: zhaozejia@szu.edu.cn

aerospace thermal systems: rough surfaces increase convective heat transfer resistance and promote boundary-layer separation, while subsurface defects (e.g., dislocations, amorphous layers) reduce thermal conductivity by scattering phonons [15, 16]. Nevertheless, single-crystal SiC exhibits extremely high hardness and chemical inertness, making its grinding and polishing challenging [17].

Currently, several polishing methods have been applied to SiC substrate processing, such as CMP [18, 19], photocatalytic-assisted chemical mechanical polishing [20], Fenton-reaction-assisted chemical mechanical polishing [21], plasma-assisted polishing (PAP) [22, 23], tribochemical polishing (TCP) [24, 25], and hydrogen etching [26, 27]. Tsai *et al*. fabricated two types of nanodiamond polishing pads (1 wt.% and 5 wt.% nanodiamond content), whose material removal rate (MRR) was approximately 2.5 times higher than that of polyurethane polishing pads [28]. Lu *et al*. developed a resin-bonded ultrafine diamond abrasive tool for Si-face machining of SiC wafers, yielding a smooth mirror-like surface with a roughness of 4.3 nm [29]. Wang *et al*. found that the synergistic effect of LPPs and photocatalysts can enhance the CMP performance of SiC [30]. Deng *et al*. employed PAP for 4H-SiC (0001) substrates, achieving atomically flat surfaces with nearly no crystal defects at the boundaries, which is critical for TPS applications requiring long-term thermal cycling reliability [31]. Yang *et al*. conducted electrochemical-mechanical polishing on a SiC surface with an initial roughness of 286 nm at a current density of 10 mA/cm² for 120 min, ultimately reducing the roughness to 1.352 nm with a MRR of 23 μm/h [32].

Molecular dynamics (MD) simulations, as an analytical tool for investigating SiC material characteristics (including defects and damage), can analyze atomic-scale kinetic processes to elucidate the atomic oxidation and removal mechanisms during CMP [33]. Tian *et al*. conducted MD simulations of scratching on the C-faces and Si-faces of 4H-SiC and 6H-SiC, finding that the amorphous deformation of the C-face was less than that of the Si-face and that scratching behavior was associated with dislocations in the SiC crystal substrate [34]. Zhou *et al*. utilized MD to investigate the surface and subsurface damage of SiC substrates polished with bonded abrasives, revealing that the exposure height and distribution density of abrasive particles significantly influence SiC material removal efficiency [35]. Sun *et al*. employed MD simulations to investigate the atomic removal mechanisms of diamond and SiO_2 abrasives on SiC surfaces during CMP, finding that SiO_2 is more prone to chemical reactions than diamond during polishing [36]. Yang *et al*. explored SiC removal in hydroxyl radical (•OH) aqueous solutions. They demonstrated that under pure chemical oxidation conditions, the adsorption of O, H, and •OH on the SiC surface forms $Si{-}OH_2$, Si−OH, $Si{-}H_2O$, and Si−H bonds, with no detachment of Si atoms. In contrast, mechanical action induces partial detachment of Si and C atoms from the substrate, forming SiO, SiO_2, CO, CO_2, or chain structures, while the remaining Si and C atoms are removed via adsorption [37].

To investigate the removal mechanism of the SiO_2 oxide layer on SiC surfaces by CeO_2 abrasives and the underlying mechanism of subsurface damage formation, MD simulations were performed to study atomic-scale material removal during CMP of the Si-face of SiC using CeO_2 abrasives. Two types of polishing slurries were formulated for Si-face polishing of SiC, and optimal process parameters were determined. Ultimately, the polished surface achieved a roughness of < 0.3 nm, providing a valuable reference for the development of high-performance SiC components for harsh aerospace environments.

2. EXPERIMENTAL

2.1. MD simulation with LAMMPS between the SiC and Abrasives

The MD simulation of the 4H-SiC polishing process was performed using LAMMPS [38]. A binning algorithm was defined every other time step to reconstruct the nearest-neighbor list. Fixed boundary conditions were applied in the z-direction to constrain wafer height variations, while periodic boundary conditions were adopted in the x- and y-directions to avoid non-physical results caused by infinite height variations [39].

Oxidizing agents, as corrosive components in the polishing slurry, chemically react with the SiC wafer surface to form a SiO_2-modified layer, which is subsequently removed by the mechanical action of abrasive particles [40]. The chemical reactions of hydrogen peroxide with SiC are presented in Equations (1)-(4), and those of potassium permanganate with SiC under acidic conditions are given in Equations (5)-(7); both reaction pathways ultimately generate an oxide layer. MD simulations were employed to realistically model material removal from SiC substrates during

CMP, incorporating the chemically generated oxide layer. This approach enabled a comparative analysis of the effects of CeO_2 abrasive particles with different radii on oxide film-coated SiC wafers.

$$2H_2O_2 \rightarrow 2H_2O + O_2 \uparrow \quad (1)$$

$$H_2O_2 \rightarrow 2 \cdot OH \quad (2)$$

$$SiC + 4 \cdot OH + O_2 \rightarrow SiO_2 + 2H_2O + CO_2 \quad (3)$$

$$SiO_2 + 2OH^- \rightarrow SiO_3^{2-} + H_2O \quad (4)$$

$$2KMnO_4 + 3H_2SO_4 \rightarrow K_2SO_4 + 3H_2O + 2MnSO_4 + 3H_2O + 5[O] \quad (5)$$

$$2MnSO_4 + 2H_2O + 5[O] \rightarrow 2Mn(OH)_2 + 2H_2SO_4 + 5[\cdot OH] \quad (6)$$

$$SiC + 4 \cdot OH + O_2 \rightarrow SiO_2 + 2H_2O + CO_2 \quad (7)$$

A 4H-SiC model with a hexagonal crystal structure was established, and its atomic regions were divided into three layers: the boundary layer (1.0 nm thick), the thermostatic layer (1.5 nm thick, located above the boundary layer), and the Newtonian layer (remaining region), as illustrated in Fig. (**1**). The combined substrate and SiO_2 oxide layer have dimensions of 22.7 × 13.1 × 8.5 nm, with crystal orientations aligned along the x-, y-, and z-directions as [1-100], [11-20], and [0001], respectively. The 4H-SiC substrate has a thickness of 7 nm, while the SiO_2 oxide layer on its upper surface is 0.5 nm thick and contains 7,800 atoms. During the polishing process, the atomic motion in the Newtonian layer was simulated using the Verlet algorithm with a time integration step of 1.0 fs. Abrasive particles were first pressed rapidly against the substrate surface along the z-axis at 2 Å/ps, followed by rotational movement at 1 Å/ps. To simulate abrasive

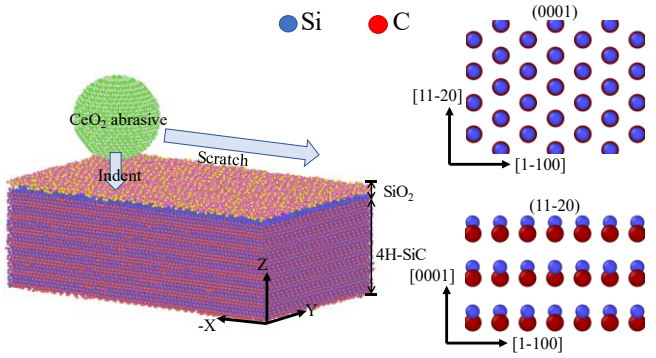

Figure 1: Molecular dynamics simulation model for nano polishing of 4H-SiC oxide layer.

particles embedded in polishing pads, three CeO_2 abrasives of different radii were used to indent and scratch the substrate. The resulting material structures were analyzed using OVITO software and characterized via the IDS method [41, 42].

In the polishing of the Si-face of SiC, to accurately describe the formation and breakage of directional bonds and analyze subsurface damage induced by mechanical action, the Tersoff potential function (Eq. (8)) [43] was selected. This potential specifically enables bond-order interaction analysis of Si-Si, C-C, and Si-C bonds within the 4H-SiC matrix. The introduction of the bij parameter and its modified attraction potential adjusts the interaction strength between atoms i and j, accounting for the influence of surrounding atoms. For the polishing of chemically generated SiO_2, the MEAM potential function (Eq. (9)) [44] was employed to model the multicomponent system (Si-C-O). This potential incorporates local atomic environmental density and angular dependence to analyze interactions between the 4H-SiC substrate and Si-O bonds. To calculate separately the interactions between CeO_2 abrasive particles and Si/C atoms on the 4H-SiC substrate, the Morse potential function (Eq. (10)) [45] was utilized. This potential simulates chemical bond breakage and formation, thereby explaining material removal behavior and abrasive wear during polishing. For the removal of the oxide layer by abrasives, the LJ/cut potential function (Eq. (11)) [46] was applied between CeO_2 abrasive atoms and Si/O atoms of the substrate. This potential is truncated at a cutoff distance $r$cut, where $V(r)$ is set to zero for $r > r_{cut}$.

$$\begin{cases} E = \sum_{i>j} f_c(r_{ij})[V_R(r_{ij}) + b_{ij} V_A(r_{ij})] \\ b_{ij} = \mu(1 + \beta^n \gamma_{ij}^n)^{-\frac{1}{2n}} \end{cases} \quad (8)$$

$$\begin{cases} E = \sum_i F_i(\rho_i) + \sum_{i \neq j} \frac{1}{2} \emptyset_j(R_{ij}) \\ F_i(\rho_i) = A_i E_i^0 \rho_i \ln \rho_i, \rho_i = \sum_{j \neq i} f(r_{ij}) \end{cases} \quad (9)$$

$$V(r) = \sum_{i<i} \varepsilon \left[e^{-2\alpha(r-r_0)} - 2e^{-\alpha(r-r_0)} \right], r < r_c \quad (10)$$

$$V(r) = \sum_{i<i} 4\varepsilon \left[\left(\frac{\sigma}{r}\right)^{12} - \left(\frac{\sigma}{r}\right)^{6} \right] \quad (11)$$

Prior to the polishing simulation, the NVT ensemble was used to gradually raise the model temperature from 0 K to 300 K [47]. The system was energy-minimized and equilibrated at 300 K for 500 ps to obtain a stable configuration. Following equilibration, polishing of the 4H-SiC substrate was initiated. During the simulation, the thermostatic layer achieved precise

temperature control via the NVT ensemble, while the NVE ensemble was adopted for the remaining layers (excluding the fixed boundary layer) to preserve microcanonical dynamics. To ensure mechanical stability, the bottom boundary layer was rigidly constrained, effectively preventing substrate displacement during polishing. Concurrently, frictional heat generated within the Newtonian layer was efficiently dissipated using a Berendsen thermostat, guaranteeing continuous thermal equilibrium at 300 K throughout the simulation.

2.2. Materials and Characterizations

4H-SiC substrates (diameter: 6 inches, thickness: 350 μm) were polished on an AMAT REFLEXION polisher using a polyurethane SUBA 800 polishing pad. To determine the optimal process parameters, two CeO_2-based slurries were prepared by mixing ACTL-AD100 ceria slurry (abrasive concentration: 39 wt%, average particle size: 20 nm, pH 6.0) with $KMnO_4$ solution at volume ratios of 1:10 and 1:20. Each CMP experiment was conducted for 60 min or 120 min under the following conditions: an applied pressure of 4 psi, a slurry flow rate of 150 mL/min, and platen/head rotational speeds of 87 rpm/118 rpm (full parameters are provided in Table **1**). After polishing, the SiC substrates were subjected to sequential ultrasonic cleaning with deionized water, H_2SO_4, and H_2O_2 for 20 min, followed by rinsing with anhydrous ethanol and subsequent thorough air drying.

Table 1: Polishing Experimental Parameters.

Process Parameters	Conditions
Substrate	4H–SiC, 6-inch
Polisher	AMAT REFLECTION
Pad	Polyurethane SUBA 800
Pressure	4 psi
Slurry flow rate	150 mL/min
Platen/head speed	87/118 rpm
Polishing time	20/60/120 min

The abrasive properties of the slurry were characterized using an FEI Scios scanning electron microscope (SEM), a JEM-F200 transmission electron microscope (TEM), and an energy dispersive spectrometer (EDS). The surface morphology and roughness of polished SiC wafers were measured using an MTP-3DInfinify atomic force microscope (AFM) (test area: 10 μm×10 μm) and a Bruker Contour GT-K white light interferometer.

3. RESULTS AND DISCUSSION

3.1. Molecular Dynamics Simulation of Chemical-Mechanical Polishing with Abrasive Particles of Different Particle Sizes

Fig. (**2**) depicts the spatial temperature distribution within the deformation zone of the 4H-SiC matrix after scratching with CeO_2 abrasives of three distinct radii (2 nm, 2.5 nm, and 3 nm), supplemented by a quantitative curve illustrating temperature variation across the scratch region. Panels (a)-(c) of the figure reveal that high-temperature domains are exclusively localized in the vicinity of the abrasive-substrate contact interface, with both lateral and vertical extents of these domains expanding monotonically as abrasive radius increases. For example, the high-temperature region (>600 K) induced by the 3 nm radius abrasive (Fig. **2c**) exhibits a lateral width approximately 2 times larger than that induced by the 2 nm abrasive (Fig. **2a**). The quantitative plot in Panel (d) further quantifies this trend: with a nonlinear temperature elevation observed as abrasive radius increases. In contrast, low-temperature regions (<400 K) remain confined to the subsurface (>5 nm below the contact interface) across all abrasive size conditions. This radius-dependent temperature variation arises from two effects. First, larger abrasives generate a larger contact area between the abrasive and 4H-SiC substrate, which intensifies plastic deformation of the 4H-SiC lattice-this deformation process dissipates significant energy through dislocation motion and grain boundary sliding, converting mechanical energy into thermal energy. Second, the frictional energy input at the abrasive-substrate interface exceeds the heat dissipation capacity of 4H-SiC, leading to cumulative heat accumulation in the contact region. In contrast, smaller abrasives mitigate this thermal buildup by reducing both the contact area and the frictional shear stress at the interface, thereby limiting energy dissipation and heat retention. In aerospace environments, Hypersonic TPS components experience transient temperature spikes up to 1800℃, and subsurface defects induced by excessive polishing temperatures can act as initiation sites for thermal cracking during thermal cycling [48]. Specifically, the localized temperature peaks (>850 K) observed with abrasives larger than 2 nm (Fig. **2d**) align with literature findings that SiC lattice stability degrades at temperatures exceeding 800 K, promoting oxidation and grain boundary weakening. Minimizing polishing-induced temperature elevation is therefore beneficial to preserving the high-temperature structural performance of SiC—excessive thermal

damage during processing impairs the material's ability to withstand repeated exposure to extreme aerothermal loads [49, 50].

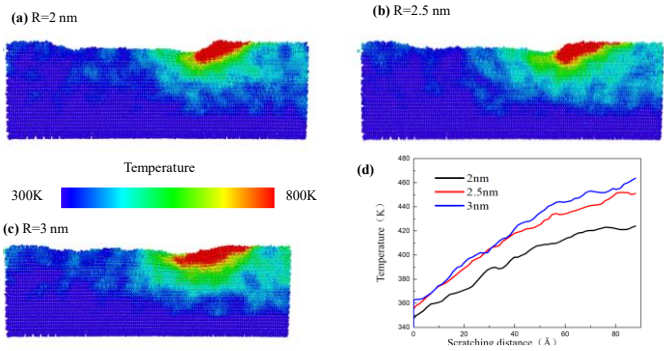

Figure 2: Temperature distribution on the substrate surface after abrasive grit scratching with different radii. (a) Radius R=2nm. (b) Radius R=2.5nm. (c) Radius R=3nm. (d) Temperature variation plot.

Fig. (**3**) presents the atomic displacement distribution of 4H-SiC in both the x-y (planar) and x-z (cross-sectional) planes following polishing with CeO_2 abrasives of 2 nm, 2.5 nm, and 3 nm radii. A clear trend emerges wherein the width of the scratch trajectory, defined by atomic displacement, expands in direct correspondence with the increasing abrasive particle radius. Regions of maximum atomic displacement are consistently localized at the leading edge of the abrasive particle, within the primary scratch groove, and along its lateral peripheries. This observation signifies that a larger abrasive radius induces more severe substrate surface deformation. During the polishing process, atomic displacements initially increase as the 4H-SiC substrate undergoes compression. However, as the abrasive particle traverses past a given point, the substrate surface undergoes a degree of elastic recovery in the vertical direction, leading to a partial reduction in the final

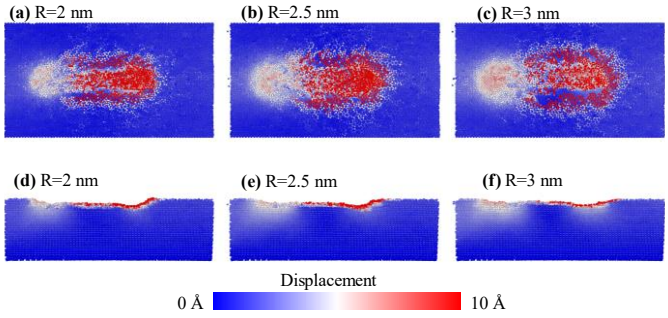

Figure 3: Atomic displacement distribution on the surface and subsurface of the 4H-SiC matrix under abrasive scratches with different radii.

atomic displacement within the indented region. This correlation between abrasive size and the extent of atomic displacement is fundamental to understanding the mechanical aspect of material removal and residual stress formation. The observed elastic recovery is a critical factor influencing the final surface topography, a phenomenon also highlighted in studies on dislocation behavior in 4H-SiC [51].

Fig. (**4**) analyzes the cross-sectional (y-[11-20] direction) structural transformations of 4H-SiC following polishing with different-sized abrasives, classifying atoms into three distinct categories: crystalline (maintaining hexagonal or cubic diamond lattice structure), amorphous (exhibiting short-range order but long-range disorder [52]), and "other" (surface-extruded stacked atoms resulting from abrasive plowing). Notably, amorphous atoms are consistently localized at the apex of scratch grooves, forming a continuous thin layer that adheres to the groove surface-this spatial distribution is invariant with abrasive radius, while the layer's thickness and volume fraction exhibit significant size dependence. Quantitative analysis demonstrates an abrasive radius-dependent increase in "other"-type atoms, indicating more severe amorphous transformation and enhanced subsurface damage during polishing with larger abrasives. The subsurface damage layer thickness, determined from vertical amplitude variations in the amorphous region, exhibits a positive correlation with abrasive radius. Furthermore, progressive lattice disruption is evidenced by the decreasing proportion of hexagonal and cubic diamond crystalline atoms in the 4H-SiC matrix as abrasive size increases. These structural degradations occur both beneath the amorphous damage layer and along the advancing edge of the polishing trajectory. The radius-dependent structural transformation arises from the stress-induced disruption of Si-C covalent bonds, when larger abrasives generate a higher contact pressure that exceeds the yield strength of 4H-SiC. This excessive pressure triggers two key processes: first, extensive dislocation glide along the (0001) basal plane, which breaks the long-range lattice order by shifting atomic layers out of alignment; second, the dissociation of Si-C bonds under shear stress, which converts the ordered crystalline structure into a disordered amorphous phase. The amorphous layer acts as a "mechanical buffer" that facilitates material removal by reducing the abrasive-substrate friction coefficient, but its increased thickness for larger abrasives introduces subsurface damage. During the CMP process, high stress concentrations and localized

high temperatures induced by larger abrasives trigger irreversible amorphous transformation of the 4H-SiC lattice, thereby forming a structurally disordered amorphous thin layer in the subsurface region—a phenomenon that potentialy impedes efficient heat transfer. This subsurface defect layer acts as an interfacial thermal resistance layer, which notably increases device thermal resistance and obstructs the effective conduction of heat from the active region to the heat sink [53]. Optimizing the CMP process to reduce the depth of subsurface damage to less than 1 nm may eliminate this thermal resistance effect, which in turn ensures that SiC materials retain their intrinsic high thermal conductivity in the harsh high-thermal-gradient environments of aerospace applications, thereby guaranteeing that components attain optimal heat dissipation efficiency and optimal thermal management capability [54].

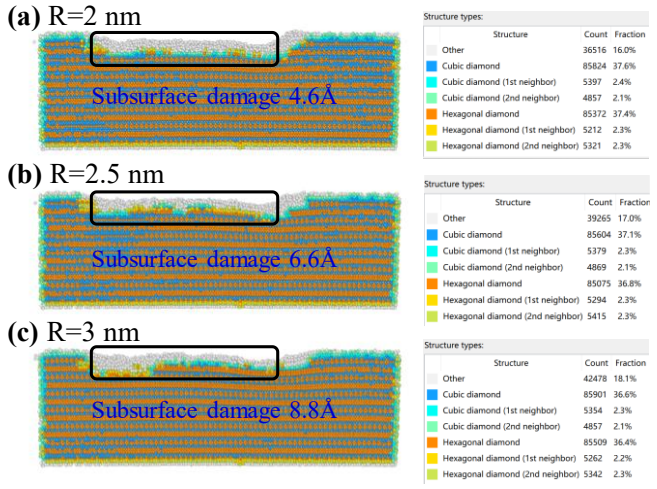

Figure 4: Surface and sub-surface damage of 4H-SiC substrate under abrasive scratches of different radii.

Fig. (**5**) presents the von Mises stress distributions in 4H-SiC matrix atoms following polishing with varying abrasive radii, integrating both spatial mapping and quantitative analysis, and visualized through atomic coloration based on established stress analysis principles [55]. Figs. (**5a-c**) illustrates the x-y planar stress distributions, while Figs. (**5d-f**) displays the corresponding x-z planar configurations. Notably, high-stress concentrations are strictly confined to the circular contact area between the abrasive and substrate, with the diameter of this high-stress zone expanding linearly with abrasive radius, and the maximum stress values localized 1-2 nm below the contact interface. Quantitative analysis demonstrates a significant 49% increase in the average surface stress, rising from 13.5 GPa to 20.1 GPa, as the abrasive radius is increased from 2 nm to 3 nm. This trend is attributed to enhanced strain-induced hardening mechanisms under larger abrasive contact areas [56], as evidenced by the progressive expansion of high-stress domains correlating with abrasive size. The observed stress amplification is inversely correlated with crystalline phase stability, suggesting that elevated contact stresses not only intensify subsurface lattice distortion but may also influence wear resistance through localized densification effects. Residual stresses and subsurface damage—such as amorphous layers and micro-dislocations—are prone to act as preferential sites for fatigue crack nucleation and propagation under subsequent thermal cycling or high-temperature, high-stress conditions, which may compromise the structural integrity and service life of SiC components [57, 58]. Furthermore, stress concentrations and pre-existing defects can undermine the uniformity and compactness of the silica protective layer, which may weaken the ability of SiC materials to withstand thermomechanical fatigue and creep when used as thermal protection systems or engine components under extreme operating conditions [59].

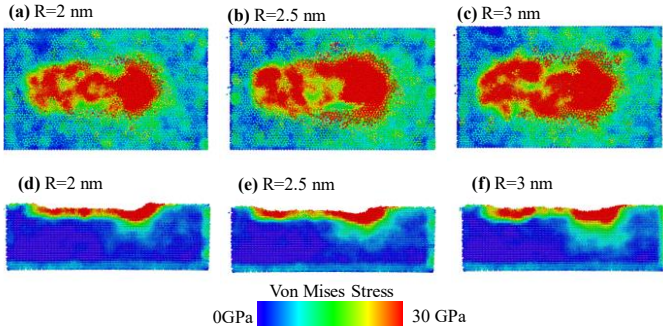

Figure 5: Stress distribution on the surface and sub-surface of 4H-SiC matrix with different radius abrasive scratches.

3.2. COMPARISON OF THE POLISHING EFFECT OF TWO DIFFERENT TYPES OF POLISHING SLURRIES

Fig. (**6**) provides a comprehensive microstructural and compositional characterization of CeO_2 slurry. SEM analysis of CeO_2 polishing slurry revealed abrasive particles with an average diameter of 20 nm (Fig. **6a**), and Fig. (**6b**) demonstrated superior colloidal stability, as evidenced by the homogeneous dispersion of CeO_2 abrasives at the 0.5 μm scale without observable agglomeration. This uniform spatial distribution effectively mitigates scratch formation and interfacial stress inhomogeneity during tribological interactions. Further nanoscale investigation via TEM (Figs. **6c-d**) identified the individual CeO_2 abrasives in slurry B as elliptically shaped nanoparticles with a

mean major axis length of 20 nm. This oblate geometry enhances surface contact efficiency while minimizing localized stress concentrations, thereby optimizing material removal uniformity. EDS quantified the elemental composition, yielding a cerium-to-oxygen mass ratio of 74.81 wt% Ce and 25.19 wt% O. These values align with the theoretical stoichiometry of cerium dioxide, confirming the phase purity and chemical integrity of the abrasive system. The superior performance of slurry B can be attributed to these characteristics; the homogeneous dispersion prevents scratch formation from agglomerates, while the small, elliptical morphology of the 20 nm nanoparticles enhances surface contact efficiency and minimizes localized stress concentrations, thereby optimizing removal uniformity. This aligns with the MD simulation results, which predict that smaller abrasives mitigate defect generation.

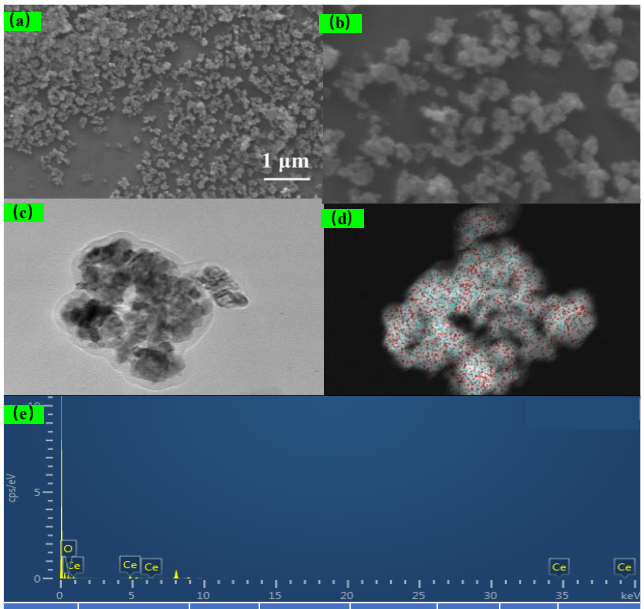

elemental	line type	k-factor	k Factor type	absorption correction	wt%	wt% Sigma	Atomic percentage
O	K-line system	1.455	theoretical	1.00	25.19	0.92	74.67
Ce	L-line system	2.060	theoretical	1.00	74.81	0.92	25.33
total:					100.00		100.00

Figure 6: Characterization results of CeO_2 polishing slurry. (a)-(b) SEM image, (c)-(d) TEM image, (e) EDS spectrum.

Fig. (**7**) presents the results of single-factor experiments analyzing the influence of polishing pressure and rotational speed on surface topography, guided by the principles of Preston's equation [60]. Figs. (**7a-c**) present the AFM morphologies of samples polished under applied pressures of 3, 4, and 5 psi, respectively. And Figs d-f display the corresponding AFM morphologies obtained under rotational speeds of the polishing platen at 98, 108, and 118 rpm, respectively. As the polishing pressure increases, the surface roughness of the polished 4H-SiC tends to increase correspondingly. A similar trend is observed with rising rotational speed of the polishing pad. This phenomenon can be primarily attributed to the direct influence of polishing pressure and rotational speed on the contact force between abrasive particles and the wafer surface, which in turn significantly affects material removal efficiency and surface morphology. Although higher polishing pressure enhances the material removal rate, it also intensifies mechanical interactions at the wafer surface, thereby increasing the likelihood of surface defects such as scratches and pits.

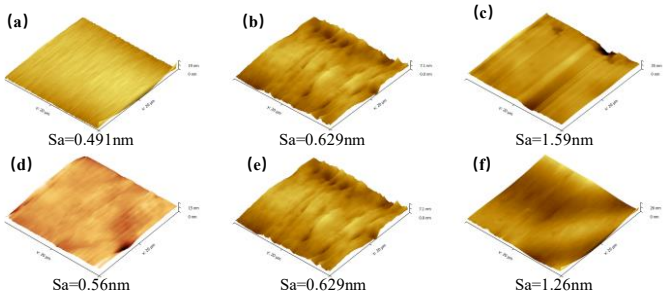

Figure 7: Single-factor experiment with speed and pressure.

Fig. (**8**) illustrates the distinctive surface morphology of the 4H-SiC substrate achieved through an optimized two-stage polishing process. Specifically, initial rough planarization was performed using a diluted CeO_2 polishing slurry with a CeO_2: H_2O_2 ratio of 1:20 for a duration of 60 minutes, followed by a diluted CeO_2 polishing slurry with a CeO_2: $KMnO_4$ ratio of 1:20 for subsequent fine polishing, with periodic replenishment of $KMnO_4$ solution. Atomic force microscopy analysis over a 10×10 μm² scanning area (Fig **8a-b**) revealed an arithmetic mean surface roughness (Sa) of 0.157 nm, with complete elimination of surface grooves. MD simulations indicate that when the ratio of silicon oxide layer thickness to abrasive particle size (d/D ≈0.1) exceeds a critical threshold, abrasive ploughing is effectively suppressed. Under these conditions, interfacial shear stress dominates over mechanical indentation, promoting bonding and delamination of the oxide layer rather than inducing microcracks via brittle fracture. Additionally, the chelating agent present in the polishing solution mitigates the anisotropy of chemical etching, thereby ensuring uniform material removal along the (0001) crystal plane and preventing defect formation. The two-stage polishing strategy adopted in this study achieved atomic-level surface roughness (Sa = 0.157 nm) and minimal subsurface damage (depth <

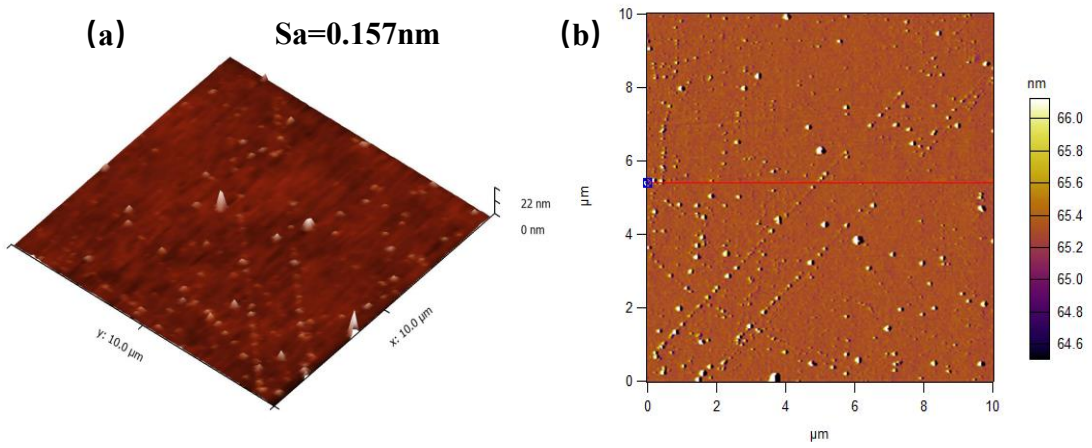

Figure 8: AFM images, (a) Surface topography image, (b) 2D areal surface image.

1 nm), minimizing stress concentration points and dislocation defects in the SiC lattice and ensuring higher chemical uniformity and structural integrity of the SiC surface. It also promoted the formation of a dense and uniform SiO_2 protective layer during its service in high-temperature aerospace environments. This not only may enhance the oxidation stability and surface durability of SiC components, thereby ensuring their structural reliability under thermal shock and long-term high-temperature service conditions, but also that ultra-low surface roughness can reduce the frictional resistance at the interface between the surface and high-speed airflow, thereby lowering aerodynamic resistance and related aerothermal loads [60].

Fig. (**9**) provides atomic-level structural characterization of the polished wafer. Fig (**9a**) presents a high-resolution aberration-corrected HAADF-STEM image of the polished 4H-SiC wafer surface, revealing a uniform lattice structure without discernible dislocation lines. This indicates that mechanical stresses during polishing remained within the material's elastic limit, thereby preventing plastic deformation and dislocation formation. Additionally, chemical components in the polishing slurry likely formed a protective surface film, further minimizing the impact of mechanical stresses on the structural integrity of the subsurface region. Fig (**9b**) shows a field-emission FE-TEM image of the polished 4H-SiC wafer, demonstrating the absence of detectable subsurface damage to a depth of approximately 5 nm below the surface. This suggests that stress wave propagation generated during polishing was effectively suppressed within the bulk material, inhibiting the development of subsurface defects. The suppression of subsurface damage is further attributed to the $KMnO_4$ replenishment strategy, which enables a synergistic chemical-mechanical effect. Specifically, the periodic introduction of fresh oxidizers enhances the dynamic redox equilibrium at the polishing interface, promoting uniform material removal and facilitating the passivation of surface defects. The atomic-level structural characterization of the polished wafer reveals no obvious dislocation lines or detectable subsurface damage, which minimizes residual stress and defects (such as dislocations and amorphous layers) in the subsurface lattice. These defects and high stress concentration regions are the main sources of crack initiation. Under the coupled effect of high thermal gradients and mechanical stress, they cause thermal stress concentration and accelerate the propagation of fatigue cracks, thereby affecting the thermal shock resistance and service life of SiC components. The atomically smooth surface minimizes subsurface damage, enhances the uniformity of heat conduction, and avoids stress concentration caused by local hotspots. This may be beneficial for the long-term oxidation stability of SiC under high thermal gradient conditions, thereby ensuring the reliability and structural integrity of SiC in thermal protection systems and propulsion components [61].

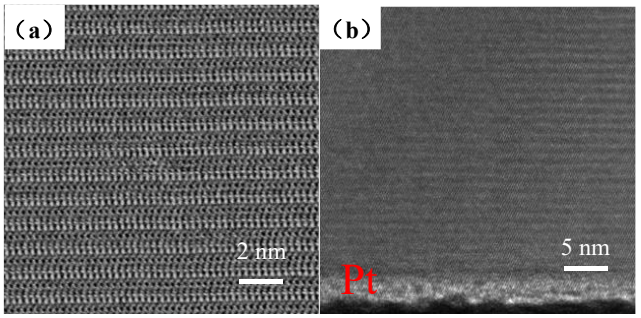

Figure 9: Atomic-level structural characterization of the polished wafer. (a) Aberration-corrected HAADF-STEM dark-field image, (b) FE-TEM bright-field image.

4. CONCLUSION

This study systematically investigates atomic-scale material removal mechanisms and process optimization in CeO_2-abrasive-based CMP of 4H-SiC through integrated MD simulations and experimental validation. The principal findings are summarized as follows:

1. MD simulations revealed the influence of abrasive radius on polishing dynamics: larger abrasives (2-3 nm radius) induce localized temperature peaks exceeding 850 K, promoting lattice softening and amorphous-phase transformation. TEM analyses demonstrated that increasing abrasive size correlates with higher dislocation density and thicker subsurface amorphous layers (3-5 nm depth). Irreversible amorphous transformations were found to dominate material removal, accounting for over 85% of atomic displacements, with amorphous-phase atoms preferentially accumulating at scratch groove apexes-identified as critical nucleation sites for subsurface damage under cyclic loading.

2. Experimental results established a direct correlation between abrasive particle size and surface defect severity. FE-TEM characterization confirmed that sub-20 nm CeO_2 abrasives significantly reduced scratch depth variation, with the near-absence of dislocations and minimal subsurface lattice distortions (deviation< 0.5 nm) under optimized conditions, indicating that nanoscale abrasives enhance removal uniformity while mitigating stress concentration.

3. Parametrically optimized CMP conditions-4 psi applied pressure, 87/108 rpm head/platen rotational speeds, and 150 mL/min slurry flow rate-achieved atomic-level surface finish via a two-stage polishing process. Stage 1 (0-60 min): CeO_2 slurry (CeO_2: H_2O_2 ratio of 1:20) reduced initial Sa roughness through aggressive planarization. Stage 2 (after 60 min): CeO_2 slurry (CeO_2: $KMnO_4$ ratio of 1:10) with periodic replenishment achieved an ultra-low Sa value of 0.157 nm, enabled by defect-passivated precision polishing.

4. Mechanistic analysis confirms that controlled oxidative etching-facilitated by H_2O_2/$KMnO_4$ redox cycling combined with tailored abrasives effectively decouples MRR from surface damage generation. This approach achieves a balance between chemical passivation and mechanical wear, thereby establishing a non-destructive polishing protocol for high-quality surface finishing of 4H-SiC substrates. The ultra-smooth surface is beneficial to hypersonic thermal protection systems by suppressing the transition from laminar to turbulent boundary layers, which may reduce the thermal contact resistance of avionics components and ensure uniform heat conduction across the system.

ACKNOWLEDGEMENTS

The work described in this paper was jointly supported by the National Natural Science Foundation of China (Grant No. 52205489), the Shenzhen Basic Research General Program (No. JCYJ20240813142312017) and the Jiangsu Key Laboratory of Precision and Micro-Manufacturing Technology (Project No. JSKL2223K09).

REFERENCES

[1] Hossain N, Mobarak MH, Mimona MA, Islam MA, Hossain A, Zohura FT, *et al*. Advances and significances of nanoparticles in semiconductor applications–A review. Results in Engineering. 2023;19:101347.

[1] Lebedev A, Chelnokov V. Wide-gap semiconductors for high-power electronics. Semiconductors. 1999;33(9):999-1001.

[2] Langpoklakpam C, Liu A-C, Chu K-H, Hsu L-H, Lee W-C, Chen S-C, *et al*. Review of silicon carbide processing for power MOSFET. Crystals. 2022;12(2):245.

[3] Dzurak A. Diamond and silicon converge. Nature. 2011;479(7371):47-8.

[4] Madar R. Silicon carbide in contention. Nature. 2004;430(7003):974-5.

[5] Liu L, Yang L, Ma H, Luo J, Xiao X, Zhao C, *et al*. Oxidation induced emissivity evolution of silicon carbide based thermal protection materials in hypersonic environments. Journal of Asian Ceramic Societies. 2021;9(4):1506-15.

[6] Hornberger J, Mounce S, Schupbach R, McPherson B, Mustain H, Mantooth A, *et al*. High-temperature integration of silicon carbide (SiC) and silicon-on-insulator (SOI) electronics in multichip power modules (MCPMs). 2005 European conference on power electronics and applications: IEEE; 2005. p. 10 pp.-P. .

[7] Takahashi Y, Yamada K, Abe T, Suzuki K. Aerodynamic heating around flare-type membrane inflatable vehicle in suborbital reentry demonstration flight. Journal of spacecraft and rockets. 2015;52(6):1530-41.

[8] Lang F, Yamaguchi H, Sato H. Package reliability of the SiC power modules in harsh environments. Additional Papers and Presentations. 2011;2011(HITEN):000139-44.

[9] Bahman AS, Iannuzzo F, Blaabjerg F. Mission-profile-based stress analysis of bond-wires in SiC power modules. Microelectronics reliability. 2016;64:419-24.

[10] Zheng P, Zhao. Progress of the new generation SiC power electronic devices. Semiconductor Technology. 2013;38(2):81-8.

[11] Wang S-Z, Xu L-Y, Shu B-Y. Physical properties, bulk growth, and applications of SiC single crystal. Jornal of Inorganic Materials-Beijing-. 1999;14:527-34.

[12] Lu J, Wang Y, Luo Q, Xu X. Photocatalysis assisting the mechanical polishing of a single-crystal SiC wafer utilizing an

anatase TiO2-coated diamond abrasive. Precision Engineering. 2017;49:235-42.

[13] Yang G, Feihu Z. Review on formation mechanism of chemical reaction layer during chemical mechanical polishing of monocrystalline SiC and sapphire substrates. Chinese Science Bulletin. 2016;61(36):3930-9.

[14] Santamore D, Cross M. Effect of phonon scattering by surface roughness on the universal thermal conductance. Physical review letters. 2001;87(11):115502.

[15] Hopkins PE. Thermal transport across solid interfaces with nanoscale imperfections: effects of roughness, disorder, dislocations, and bonding on thermal boundary conductance. International Scholarly Research Notices. 2013;2013(1):682586.

[16] Jiang Z-y, Ye G, Jian J. Mechanical properties of SiC whiskers reinforced SiCf/SiC composites. Journal of Materials Engineering. 2021;49(8):89-96.

[17] Singh RK, Bajaj R. Advances in chemical-mechanical planarization. MRS bulletin. 2002;27(10):743-51.

[18] Song X, LI Y, Jiang N, Qu Y, Qiu G. Recent development of chemical mechanical polishing. Chemical industry and engineering progress. 2008;27(1):26.

[19] Luo Q, Wen H, Lu J. Sol–gel polishing technology for extremely hard semiconductor substrates. The International Journal of Advanced Manufacturing Technology. 2022;120(3):1415-32.

[20] Xia Y, Chen G, Ni Z, Wang H, Qian S, Bian D. Effect of photo-Fenton reaction on chemical mechanical polishing of 6H-SiC. Lubrication Engineering. 2021;46(1):74-9.

[21] Deng H, Ueda M, Yamamura K. Characterization of 4H-SiC (0001) surface processed by plasma-assisted polishing. The International Journal of Advanced Manufacturing Technology. 2014;72(1):1-7.

[22] Yamamura K, Takiguchi T, Ueda M, Deng H, Hattori A, Zettsu N. Plasma assisted polishing of single crystal SiC for obtaining atomically flat strain-free surface. CIRP annals. 2011;60(1):571-4.

[23] Lin Y, Kao C. A study on surface polishing of SiC with a tribochemical reaction mechanism. The International Journal of Advanced Manufacturing Technology. 2005;25(1):33-40.

[24] Zhu Z, Muratov V, Fischer TE. Tribochemical polishing of silicon carbide in oxidant solution. Wear. 1999;225:848-56.

[25] Ramachandran V, Brady M, Smith A, Feenstra R, Greve D. Preparation of atomically flat surfaces on silicon carbide using hydrogen etching. Journal of Electronic Materials. 1998;27(4):308-12.

[26] Owman F, Hallin C, Mårtensson P, Janzen E. Removal of polishing-induced damage from 6H-SiC (0001) substrates by hydrogen etching. Journal of crystal growth. 1996;167(1-2):391-5.

[27] Tsai M, Wang S, Tsai C, Yeh T. Investigation of increased removal rate during polishing of single-crystal silicon carbide. The International Journal of Advanced Manufacturing Technology. 2015;80(9):1511-20.

[28] Lu J, Luo Q, Mao X, Xu X, Wang Y, Guo H. Fabrication of a resin-bonded ultra-fine diamond abrasive polishing tool by electrophoretic co-deposition for SiC processing. Precision Engineering. 2017;47:353-61.

[29] Wang W, Zhang B, Shi Y, Zhou J, Wang R, Zeng N. Improved chemical mechanical polishing performance in 4H-SiC substrate by combining novel mixed abrasive slurry and photocatalytic effect. Applied Surface Science. 2022;575:151676.

[30] Deng H, Yamamura K. Atomic-scale flattening mechanism of 4H-SiC (0 0 0 1) in plasma assisted polishing. CIRP annals. 2013;62(1):575-8.

[31] Yang X, Yang X, Kawai K, Arima K, Yamamura K. Highly efficient planarization of sliced 4H–SiC (0001) wafer by slurryless electrochemical mechanical polishing. International Journal of Machine Tools and Manufacture. 2019;144:103431.

[32] Man Q, Sun Q, Wang Y, Xu J. Atomistic Removal Mechanisms of SiC in Hydrogen Peroxide Solution. Micromachines. 2024;15(6):754.

[33] Tian Z, Chen X, Xu X. Molecular dynamics simulation of the material removal in the scratching of 4H-SiC and 6H-SiC substrates. International Journal of Extreme Manufacturing. 2020;2(4):045104.

[34] Zhou P, Shi X, Li J, Sun T, Zhu Y, Wang Z, *et al*. Molecular dynamics simulation of SiC removalmechanism in a fixed abrasive polishing process. Ceramics international. 2019;45(12):14614-24.

[35] Sun Q, Xu J, Lu k, Zhu Z. Microscopic simulation analysis on function of diamond and silica particles during chemical mechanical polishing of silicon carbide. Electroplating & Finishing. 2021;40(16):1254-61. doi: 10.19289/j.1004-227x.2021.16.005.

[36] Yang S, Li X, Zhao Y, Al-amin M, Grøndahl L, Lu M, *et al*. MD simulation of chemically enhanced polishing of 6H-SiC in aqueous H2O2. Journal of Manufacturing Processes. 2023;107:515-28.

[37] 38. Thompson AP, Aktulga HM, Berger R, Bolintineanu DS, Brown WM, Crozier PS, *et al*. LAMMPS-a flexible simulation tool for particle-based materials modeling at the atomic, meso, and continuum scales. Computer physics communications. 2022;271:108171.

[38] Wang B, Kang G, Wu W, Zhou K, Kan Q, Yu C. Molecular dynamics simulations on nanocrystalline super-elastic NiTi shape memory alloy by addressing transformation ratchetting and its atomic mechanism. International Journal of Plasticity. 2020;125:374-94.

[39] Zhang Y, Zhang L, Chen K, Liu D, Lu D, Deng H. Rapid subsurface damage detection of SiC using inductivity coupled plasma. International Journal of Extreme Manufacturing. 2021;3(3):035202.

[40] Zhou P, Li J, Wang Z, Chen J, Li X, Zhu Y. Molecular dynamics study of the removal mechanism of SiC in a fixed abrasive polishing in water lubrication. Ceramics International. 2020;46(16):24961-74.

[41] Stukowski A. Visualization and analysis of atomistic simulation data with OVITO–the Open Visualization Tool. Modelling and simulation in materials science and engineering. 2009;18(1):015012.

[42] Shi L, Ma X, Li M, Zhong Y, Yang L, Yin W, *et al*. Molecular dynamics simulation of phonon thermal transport in nanotwinned diamond with a new optimized Tersoff potential. Physical Chemistry Chemical Physics. 2021;23(14):8336-43.

[43] Mandal D, Shukla KA, Ghosh A, Gupta A, Dhabliya D. Molecular dynamics simulation for serial and parallel computation using leaf frog algorithm. 2022 Seventh International Conference on Parallel, Distributed and Grid Computing (PDGC): IEEE; 2022. p. 552-7.

[44] Bétermin L. Minimizing lattice structures for Morse potential energy in two and three dimensions. Journal of Mathematical Physics. 2019;60(10).

[45] Rabiee H, Hassanzadeh A, Sakhaeinia H, Alahyarizadeh G. Effect of the point defect of silicon carbide cladding on mechanical properties: a molecular-dynamics study. Chemical Papers. 2024;78(6):3815-30.

[46] Toton D, Lorenz CD, Rompotis N, Martsinovich N, Kantorovich L. Temperature control in molecular dynamic simulations of non-equilibrium processes. Journal of Physics: Condensed Matter. 2010;22(7):074205.

[47] Ng W, McNamara J, Friedmann P, Waas A. Thermomechanical behavior of damaged TPS including hypersonic flow effects. 14th AIAA/AHI space planes and hypersonic systems and technologies conference2006. p. 7951.

[48] Mazo MA, Padilla I, Tamayo A, Robla JI, López-Delgado A, Rubio J. Evaluation of thermal shock resistance of silicon oxycarbide materials for high-temperature receiver applications. Solar Energy. 2018;173:256-67.

[49] Shimoda K, Eiza N, Park J-S, Hinoki T, Kohyama A, Kondo S. High-temperature mechanical property improvements of SiC ceramics by NITE process. Materials transactions. 2006;47(4):1204-8.

[50] Li J, Yang G, Liu X, Luo H, Xu L, Zhang Y, *et al*. Dislocations in 4H silicon carbide. Journal of Physics D: Applied Physics. 2022;55(46):463001.

[51] Sreelakshmi N, Amirthapandian S, Umapathy G, David C, Srivastava S, Ojha S, *et al*. Raman scattering investigations on disorder and recovery induced by low and high energy ion irradiation on 3C-SiC. Materials Science and Engineering: B. 2021;273:115452.

[52] Ju YS, Hung M-T, Usui T. Nanoscale heat conduction across metal-dielectric interfaces. 2006.

[53] Powell JA. Chemical Mechanical Polishing of Silicon Carbide. Research and Technology 1997. 1999.

[54] Tian X, Li H, Shi X, Lin H, Yan N, Feng T. Morphologies evolution and mechanical behaviors of SiC nanowires reinforced C/(PyC-SiC) n multilayered matrix composites. Journal of Materials Science & Technology. 2022;96:190-8.

[55] Liu Y, Ji Y, Dong L, Xie H, Song J, Li J. Effect of grinding depths on SiC nanogrinding behavior based on molecular dynamics. Applied Physics A. 2022;128(1):34.

[56] Yuan G, Forna-Kreutzer JP, Xu P, Gonderman S, Deck C, Olson L, *et al*. In situ high-temperature 3D imaging of the damage evolution in a SiC nuclear fuel cladding material. Materials & Design. 2023;227:111784.

[57] Chen D, Gilbert C, Zhang X, Ritchie R. High-temperature cyclic fatigue-crack growth behavior in an in situ toughened silicon carbide. Acta materialia. 2000;48(3):659-74.

[58] Mazo MA, Padilla I, López-Delgado A, Tamayo A, Rubio J. Silicon oxycarbide and silicon oxycarbonitride materials under concentrated solar radiation. Materials. 2021;14(4):1013.

[59] Kadivar M, Azarhoushang B. Kinematics and material removal mechanisms of loose abrasive machining. Tribology and Fundamentals of Abrasive Machining Processes. William Andrew; 2022. p. 507-36.

[60] Yamaguchi S, Yusufu A, Shirahama T, Murakami Y, Onitsuka T, Uno M. High-temperature stability of SiO2 oxide film on surface of SiC. Transactions of the Atomic Energy Society of Japan. 2019;18(4):219-25.

Received on 13-11-2025 Accepted on 15-12-2025 Published on 31-12-2025

https://doi.org/10.66000/3110-9780.2025.01.09